INTERNATIONAL ATOMIC ENERGY AGENCY
UNITED NATIONS EDUCATIONAL, SCIENTIFIC AND CULTURAL ORGANIZATION
INTERNATIONAL CENTRE FOR THEORETICAL PHYSICS
I.C.T.P., P.O. BOX 586, 34100 TRIESTE, ITALY, CABLE: CENTRATOM TRIESTE

SMR.703 - 3

WORKING PARTY ON:
MECHANICAL PROPERTIES OF INTERFACES

23 AUGUST - 3 SEPTEMBER 1993

"Basic and Introductory Lectures on Fracture" (Part III)

"The Interfacial Crack in a 2D Hexagonal Lattice"

Robb THOMSON
United States Department of Commerce
National Institute of Standards and Technology
Materials Science and Engineering Laboratory
Building 223
Gaithersburg, MD 20899
U.S.A.

The Interfacial Crack in a 2D Hexagonal Lattice.

Robb Thomson*
Materials Science and Engineering Laboratory
National Institute of Standards and Technology
Gaithersburg, MD 20899

and

S. J. Zhou**
Physics Department
Washington University at St. Louis
St. Louis, MO 63130

* Supported in part by the Office of Naval Research
** Supported by the DOE Grant Number DE-FG02-84ER45130

Abstract

In this paper we compare a set of atomic calculations of interfacial crack structure and properties with the predictions of an augmented elastic theory. Our intent is to critique the elastic predictions, especially the mode conversion and displacement closure oscillation features of the elastic theory. A simple physical picture is developed based on a crack stability diagram, using two sets of stress intensity axes. The first set is the normal applied stress intensity, K, and the second is a local stress intensity factor, k, defined to describe the physics of the core region. The Griffith condition and dislocation emission criterion are defined in terms of the local k, and its associated effective core size parameter. Unfortunately, the physical core size is not a unique parameter in the problem, but varies directly with the amount of shear in the core. Thus, the effective core size for the Griffith condition is different from that for dislocation emission. In each case, the effective core size is much smaller than the physical core size, which means that the mode shift at the crack tip is considerably larger than would be expected on the basis of linear elasticity. However, with appropriately defined effective core size parameters, the Griffith condition is well satisfied, and the emission criterion based on the new Rice unstable stacking fault condition is also surprisingly well satisfied in the Mode II emission configuration. The crack is found never to exhibit displacement oscillations, in part, because of the necessary condition that the Griffith condition be satisfied at the crack tip, and in part becaus the amount of shear in the core is limited by dislocation emission.

1. Introduction

In this paper we will compare a set of atomic calculations of interfacial crack structure and properties with the predictions of the elastic continuum theory.

From its beginning, the subject of interfacial fracture has been bedeviled by the predictions of the standard theory that oscillations in displacement occur very near the crack tip[1-7]. Among the attempts to deal with this physical anomaly, Gao[8] has suggested that shear mode conversion at the tip is absorbed by a distributed dislocation contribution, which keeps the stress tensile, without oscillatory closure. There has also been work to include, explicitly, the stresses induced by the closure of the cleavage surfaces behind the crack[9]. Achenbach, etal.[10] have introduced a Barenblatt nonlinear zone at the crack tip, with the result that closure does not occur, and Knowles, etal.[11] have carried out a more extensive study of the nonlinear elastic problem with the same result. The treatments by Gao and by Achenbach, etal. are closest to our own approach, and we will discuss our results in the light of their work at the appropriate point.

We shall address the subject of closure in a realistic fashion with a crack on an interface in a 2D lattice, and show that these oscillations never occur. Beyond this, we will conduct a fairly exhaustive critique of the standard elastic continuum analysis in its most important aspects, including the mixing of stress modes at the tip, dislocation formation at the crack tip, and the fracture criterion. The result of this investigation will be a simple physical picture of the interfacial crack which is qualitatively consistent with the lattice calculations, but is couched in the terms of elasticity. That is, we shall show how to "parametrize" the elastic theory so that it is consistent with the physical requirements of the nonlinear lattice theory.

The atomic calculations will be based on the lattice Green's function analysis, which we have described earlier[12], in a simple 2D hexagonal lattice. The reason for the hexagonal lattice is that it is isotropic in the continuum elastic limit, which allows us to make a direct comparison with the analytic isotropic results for that case. The feature of the lattice Green's function approach which is unusual for this study is that it allows us to take a relatively large crack of up to 200 lattice spacings, with a cohesive zone at one end, of adjustable length, which will normally be 20 lattice positions in length, within which nonlinear forces can operate. See Fig. 1. The crack is assumed to lie on an interface between two hexagonal lattices of identical lattice structure, but with different spring constants. Further, the bonds between the upper and lower sublattices will be assumed to have a still different set of spring constants. The bonding force range will be limited to the nearest neighbor distance. We will use two forms of bond energy function, a Gaussian and a modification of the UBER of Rose, etal.[13], to be described more fully in the body of the paper. The crack is embedded in a super cell of 2000 atoms on a side, incorporating 4×10^6 atoms in total. The super cells are repeated along the x-axis parallel to the interface, thus making an infinitely long slab 2000 atoms thick. Our technique thus makes it possible to study a very large system, so that effects at the boundary, and in other neighboring super cells can be safely ignored. Further, the computations are very fast, so that exhaustive studies of the relevant parameter space can be made with ease. The details of the method for finding and using the lattice Green's functions for the interfacial system are given in our earlier paper[12]

The general motivation behind the paper is to gain generic information, and this is the reason why we use the simple hexagonal lattice with central forces limited to nearest neighbors. For this lattice we have exact analytic expressions for the isotropic continuum limit, and our model is sufficiently general to make a very severe test of this theory. A more complex model, with a lattice simulating a real bcc or fcc lattice, or with more complicated force laws would simply obfuscate the situation we wish to highlight. So our purpose is to explore the ideas underlying interfacial fracture theory, not to obtain numbers for a specific material. In this same vein, we only investigate the "Mode II" emission configuration here, in which the dislocation is emitted on the crack plane. The reason for this restriction is that Rice's unstable stacking fault criterion[14,15] is designed to work best in this configuration. Also, in this configuration, the elastic driving force for the crack is a purely tensile property, while the dislocation emission is a purely shear property, which simplifies the physics. A later study will explore the Mode I configuration, where the emission is at an angle to the cleavage plane.

In the next section, we write and extend the relevant elastic continuum equations needed in the work to follow. In §3 we propose a physical picture which rationalizes the properties of the interfacial crack in terms of an extension of the idea of a crack stability diagram which was developed for cracks in homogeneous materials under mixed loads[16]. In §4 we explain our lattice calculation technique. In §5, we report our results, and compare them with the elastic theory. Finally, we summarize the paper in §6.

2. Continuum Analysis.

We assume a crack lies on the x-axis, is centered at the origin, and extends from $x = -a$ to $x = +a$. In addition, we assume that the x-axis is also an interface between two different semi-infinite elastic media bonded to each other across the x-axis. For such a crack, the stress function written on the crack plane, $\sigma_{22}(x) + i\,\sigma_{12}(x) = \sigma(x)$, can be obtained from the analysis of Rice[6] and Rice and Sih[3], for a δ-function dipole force, $F = F_y + iF_x$ at position $x = t$, $-a < t < +a$,

$$\begin{aligned} \sigma(x) = \sigma_{22}(x) + i\,\sigma_{12}(x) &= \sqrt{\frac{a}{\pi}}\frac{K}{\sqrt{x^2-a^2}}\,\frac{a-t}{x-t}\left(\frac{x-a}{x+a}\right)^{i\epsilon} \\ K = K_I + iK_{II} &= \frac{F\,\cosh\pi\epsilon}{\sqrt{\pi a}}\sqrt{\frac{a+t}{a-t}}\left(\frac{a+t}{a-t}\right)^{i\epsilon} \\ \epsilon &= \frac{1}{2\pi}\ln\left(\frac{\kappa_1\mu_2+\mu_1}{\kappa_2\mu_1+\mu_2}\right). \end{aligned} \tag{1}$$

$\kappa = 3 - 4\nu$ for plane strain and $\kappa = (3-\nu)/(1+\nu)$ for plane stress. x is the distance from the center of the crack and μ and ν are the standard elastic constants. The complex stress intensity, $K = K_I + iK_{II}$, is slightly different from that defined by Rice[6] and Hutchinson, etal[5], and is defined here so that the stress on the crack plane near the tip has the limiting value,

$$\begin{aligned} \sigma(r) = \sigma_{22}(r) + \sigma_{12}(r) &= \frac{K}{\sqrt{2\pi r}}\,e^{i\xi} \\ \xi &= \epsilon\,\ln\left(\frac{r}{2a}\right). \end{aligned} \tag{2}$$

Here $r = x - a$ is the distance along the x-axis from the crack tip, and $r \ll a$. This definition has the standard dimensions for a stress intensity factor in homogeneous fracture mechanics.

The crack opening, δ, behind the crack, again for $|r| \ll a$, is given by[5]

$$\delta(-r) = \delta_2 + i\,\delta_1 = \frac{1}{2\mu'_{eff}(1+2i\epsilon)\cosh(\pi\epsilon)}\,K\sqrt{\frac{-r}{2\pi}}\,e^{-i\xi}\,. \tag{3}$$

The crack extension force, $\mathcal{G}$, has the standard form[4],

$$\begin{aligned}\mathcal{G} &= \frac{K\bar{K}}{2\mu'_{eff}\cosh^2(\pi\epsilon)} \\ \mu'_{eff} &= \frac{2\mu'_1\mu'_2}{\mu'_1+\mu'_2}\,,\end{aligned} \tag{4}$$

where $\mu' = \mu/(1-\nu)$ in plane strain and $\mu' = \mu(1+\nu)$ in plane stress.

To capture the central point characterizing the difference between interfacial fracture and the homogeneous case, we note that Eq. (2) predicts a phase shift between the load point and the stresses at the crack tip, so that tension at the load point rotates in the complex plane into partial shear at the crack tip. For fracture in homogeneous media, $\xi \equiv 1$, while in interfacial fracture, ξ depends on the position, r, and is singular at the tip. (There are critical values for elastic mismatch when $\xi = 1$ even in the case of interfaces, however[7].)

In the hexagonal lattice, Poisson's ratio is $\nu = 1/4$, and the shear modulus is given by $\mu = c\sqrt{3}/4$, where c is the spring constant. Note that ν is the same in both lattices, since both have the same structure. Also, in the 2D simulations, we are strictly in the plane stress limit. Thus the parameter, ϵ, is given by

$$\epsilon = \frac{1}{2\pi}\ln\left(\frac{11(c_2/c_1)+5}{11+5(c_2/c_1)}\right)\,. \tag{5}$$

In our application of these equations, the term $\cosh(\pi\epsilon)$ is always very close to unity, and will be so approximated. In the limit of very large spring constant ratios, ϵ takes the value

$$\lim_{(c_2/c_1)\to\infty}(\epsilon) = \frac{1}{2\pi}\ln(11/5) = 0.125\,. \tag{6}$$

Since oscillations in displacement can occur at atomic distances from the crack tip only when $\xi > \pi/2$, Eq. (3) predicts that our crack lengths must be (in the limiting case of large c_2/c_1) of order 2×10^5 for closure to occur, which is well beyond the capacity of our computer. In spite of this, we will find relevant crack length effects are actually well within our capacity to explore, and we shall be able to make significant comments about the oscillations problem.

To this end, we need to generalize previous notions of the Griffith and dislocation emission criteria for the interfacial case. In an earlier paper on the properties of a crack

in a homogeneous 2D hexagonal lattice[15], we found that the Griffith condition was approximately independent of the Mode II load, except for pathological force laws with large lattice trapping. We also found that for emission onto the cleavage plane (Mode II emission configuration), the criterion was approximately given by Rice's unstable stacking fault condition[14], written just for the Mode II portion of the load. That is, the two criteria for the homogeneous lattice are

$$\begin{aligned}K_{Ic} &= \sqrt{4\mu'\gamma_s} \\ K_{IIc} &= \sqrt{2\mu'\gamma_{us}}\,,\end{aligned} \tag{7}$$

where γ_s is the surface energy and γ_{us} is the unstable stacking fault. In the case of the interfacial crack, we will take as our guiding principle that the physics of the processes occuring in the core of the crack will be governed by the same local core structure and stress conditions as in the homogeneous case. One might think that because the energy release rate, $\mathcal{G}$, is independent of the phase shift, (Eq. (4)), that the phases cancel out of the problem. However, if we attempt to separate the real and imaginary portions of the stress in the core region, in keeping with our physical requirements for cleavage and emission in Eq. (7), both of these criteria become garbled by the phase shift, ξ.

The problem from the elastic standpoint is additionally complicated by the fact that there are two quite distinct and separate singularities at the tip of the interfacial crack. One is the familiar $1/\sqrt{r}$, while the other is the singularity in ξ as $r \to 0$. The definition of the complex interfacial K in Eq. (1) normalizes out both singularities in a mathematically clean manner. Keeping in mind, however, that we wish to compare the elastic theory with the lattice theory, we will instead introduce a core cut-off for the phase shift and normalize the stress intensity factor to the phase at the cut-off distance, r_0. Thus, following Gao[8], we define a new core stress intensity factor, k,

$$\begin{aligned}k &= k_I + i\,k_{II} = K\,e^{-i\xi_0} \\ \sigma_{22}(r) + i\,\sigma_{12}(r) &= \frac{k}{\sqrt{2\pi r}}\,e^{i(\xi-\xi_0)} \\ \xi_0 &= \epsilon\,\ln\left(\frac{r_0}{2a}\right),\end{aligned} \tag{8}$$

where K is the externally applied interfacial complex stress intensity defined in Eq. (1). With this form of the stress intensity factor, k_I refers to tension stresses at the core, and k_{II} refers to shear stresses there. In terms of this core-normalized stress intensity factor, we can then write postulated criteria for cleavage and dislocation emission, which automatically contain the expected phase effects at the core, and which incorporate the physical ideas which have proven to describe the critical events in homogeneous fracture. That is, we postulate that the generalized Griffith cleavage condition should be given by

$$\begin{aligned}\mathcal{G}_{Ic} &= \frac{k_{Ic}^2}{2\mu'_{eff}\cosh^2(\pi\epsilon)} = 2\gamma_s \\ k_{Ic} &= \sqrt{4\mu'_{eff}\gamma_s}\,,\end{aligned} \tag{9}$$

where γ_s is the intrinsic interfacial surface energy and $\mathcal{G}_{Ic}$ is a short hand for the square of the Mode I stress intensity factor. Likewise the Rice criterion for emission in the Mode II configuration should be given by

$$\mathcal{G}_{IIe} = \frac{k_{IIe}^2}{2\mu'_{eff}\cosh^2(\pi\epsilon)} = \gamma_{us}$$
$$k_{IIe} = \sqrt{2\mu'_{eff}\gamma_{us}}\,. \tag{10}$$

The core-normalized stress intensity factor has some of the same physical motivation behind it as the more standard difference between the applied K and the local k at the crack tip shielded by dislocations in the homogeneous lattice. For this reason, we shall refer to it simply as the local k.

3. Crack Closure and Lattice Stability.

The physical picture which results from the suggested modifications to the standard elastic theory made in the previous section is rather different from that which is now current. But it has some features which have already been anticipated by Gao[8] and by Achenbach, etal.[10]. For reasons based on this picture, we believe the "oscillations" issue is moot. Our reasons are not the standard argument that when the crack closes, then additional repulsive forces come into play to keep the material on opposite sides of the cleavage plane from overlapping[9]. Instead, there are two interconnected core structure effects which keep crack closure from ever occurring.

The first is that the crack core must always be in tension, because the atoms there must be pulled apart and physically separated in order for a crack to exist in the first place. The separation of the atoms in the core in tension is therefore a necessary condition for the existence of any atomically sharp crack, and is expressed quantitatively for the elastic crack in terms of the local k_{Ic} in Eq. (9). The elastic prediction in Eq. (3) of a closure at the core radius of the crack (at some critical value of crack length) comes about because, in pure Mode I loading, $\xi_0 \to \pi/2$, and the tensile stresses in the core also disappear. That is, the necessary condition for the existence of the crack is not satisfied.

The second crucial feature of the crack core is that as the shift angle, ξ_0, increases with growing crack length, eventually the lattice in the core breaks down in shear, and a dislocation is formed when the emission criterion in terms of the local k_{IIe} is met. Thus, as a crack grows in length, it can never achieve the condition for closure oscillations, $\xi_0 \simeq \pi/2$, but emits dislocations before this can happen.

This state of affairs can be diagramed in a simple manner by appealing to the concept of a crack stability diagram, which has been introduced for the crack in homogeneous materials[15,16]. The crack stability diagram is simply a graph of the locus of points in k_I/k_{II} space where the crack is in equilibrium. The diagram is an expression of the equilibrium dictated by Eqs. (9), (10), with an effective core size for the particular lattice and force law, and is shown in Fig. 2. Equilibrium, according to Eq. (9), is a vertical line in terms of the k_I/k_{II} axes, but our results in Ref (15), which will be confirmed for the present case in the atomic results to be reported below, show that there is some small curvature induced by k_{II}. The stability line is, however, limited by the emission points for

positive and negative dislocations at critical values of k_{II}. In Fig. 2, we have drawn the emission points as symmetric about the k_I axis, a point of some significance in the atomic results to be reported below.

The axes corresponding to the applied loading of the crack are those of K_I/K_{II}, and these axes are rotated in the complex plane by the angle, ξ_0, relative to the k_I/k_{II} axes, as shown in the figure. The rotation angle is given by Eq. (8), where r_0 is an effective core size, to be determined by the atomic calculations.

More explictly, the crack stability is diagramed, on the basis of this extended elastic theory, from Eq. (9) as the Griffith line,

$$K_{Ic}\cos\xi_0 - K_{IIc}\sin\xi_0 = 2\sqrt{\mu'_{eff}\gamma_s}, \tag{11}$$

limited by the emission points from Eq. (10),

$$K_{IIe}\cos\xi_0 + K_{Ie}\sin\xi_0 = \sqrt{2\mu'_{eff}\gamma_{us}}. \tag{12}$$

Gao[8] proposed that the Mode II shear at the crack tip be cancelled by continuous dislocation formation in the core region and subsequent shielding, leaving a pure Mode I stress at the crack tip. Under these conditions he showed that the displacement oscillations would never occur. Our finding is that the shear is not automatically cancelled at the crack tip, but that it is limited by the emission criterion. As explained above, as the phase shift angle, ξ_0 increases with crack length, dislocation emission intervenes before oscillations can occur at the point where $\xi_0 \to \pi/2$. Thus, in contrast to Gao, we find that phase shifts and shear stresses at the crack tip do occur, but are limited by the dislocation emission.

When dislocations are emitted, the shielding of the shear stresses at the crack tip will be determined by the distance to the dislocations after emission, so that the mobility of the dislocations becomes a factor in what ultimately happens at the crack tip, in addition to the mechanics of the crack by itself. That is, the local k is determined by both crack length and dislocation shielding. Dislocation shielding of interfacial cracks is a subject to which we shall return in a subsequent paper.

Achenbach, etal.[10] put a Barenblatt/Dugdale cohesive zone at the crack tip, and found solutions with no closure region. The disappearance of the closure zone is apparently due to the same physical reason that applies to us. That is, the crack is forced into Griffith equilibrium by the Barenblatt condition.

Therefore, we can summarize by saying that the oscillations are like Alice's famous Cheshire cat. The cat has gone (no oscillations), but the grin remains (stress phase shifts are real, and they are important).

We now turn to the atomic calculations, and their comparison with the predictions from the augmented elastic theory.

4. The 2D Hexagonal Model.

Once the lattice Green's functions have been determined for the cracked lattice[12], our crack modeling begins with the equation

$$\mathbf{u(l)} = \mathbf{G(l,l')F(l')} + \mathbf{G(l,l')f\{l'\}}\,, \tag{13}$$

where $\mathbf{u}(\mathbf{l})$ is the vector displacement of the lattice point at $\mathbf{l}$, and $\mathbf{G}(\mathbf{l},\mathbf{l}')$ is the Green's function for the lattice field point, $\mathbf{l}$, and source point, $\mathbf{l}'$. $\mathbf{F}(\mathbf{l}')$ is the external vector force dipole applied on the crack open surface at the lattice position $\mathbf{l}'$. (That is, the force is applied in opposite directions to atoms facing one another across the cleavage plane at position $\mathbf{l}'$.) $\mathbf{f}\{\mathbf{l}'\}$ is the vector force functional acting on the lattice point $\mathbf{l}'$ due to the nonlinear bonds connecting that atom to its neighbors.

In our case, as noted in the Introduction, the force will be assumed to be a simple central pair force between nearest neighbors. We will use two forms of this force. The first is that proposed by Rose, *etal.*[13], modified so that the force goes smoothly to zero at the cut-off distance, which we take to be the next nearest neighbor distance. This force is given by

$$\begin{aligned} f(u) &= -\frac{cu}{1-a}\left(e^{-u/\alpha} - a\right) \\ a &= e^{-(\sqrt{3}-1)/\alpha}\ , \end{aligned} \tag{14}$$

where the force is directed on the line between the two atoms, and u is the displacement of the two atoms from their equilibrium radial distance from one another. c is the spring constant, and α is the range of the force. The bond energy, $U(u)$, of such a bond is

$$\begin{aligned} U(u) &= -\frac{c}{1-a}\left(\alpha(u+\alpha)e^{-u/\alpha} + \frac{a}{2}u^2\right) - U_0 \\ U_0 &= -\frac{ca}{1-a}\left(\alpha(\alpha+\sqrt{3}-1) + \frac{(\sqrt{3}-1)^2}{2}\right)\ . \end{aligned} \tag{15}$$

The bond strength is $E_b = -c\alpha^2/(1-a) - U_0 = \gamma_s$, where γ_s is the surface energy. The surface energy per lattice spacing is composed of two bonds for the hexagonal lattice (see Fig. 1). Both of these equations, and all our subsequent work, are normalized in terms of unit lattice spacing. In the following, we will standardize on a bond strength of $E_b = 0.04c$, which is the bond strength for Copper in the normalized units when $c = 1$. The second force law, again a nearest neighbor central pair force, is the Gaussian law,

$$\begin{aligned} f(u) &= -cu\, e^{-u^2/\beta} \\ U(u) &= -\frac{c\beta}{2}\, e^{-u^2/\beta}\ , \end{aligned} \tag{16}$$

Here, β is the range, and the bond strength is $E_b = c\beta/2$.

In all simulations, we will normalize the lower lattice to have spring constant $c_1 = 1$. The upper spring constant is c_2, and the interfacial spring constant connecting the two lattices is c_{12}. Since only the interface will be separated, we need to know the energy function for the bonding between the two lattices, not the intra-lattice bonding. That is, we assume the upper and lower lattices always remain in their linear regimes. This assumption requires all the "action" to take place on the cleavage plane ahead of the crack. So no branching of the crack and no dislocation emission off the cleavage plane is allowed.

As noted in the Introduction, the system we start with is a super cell composed of 4×10^6 lattice points. When the interface is constructed along the horizontal x-axis, the periodicity in the y-direction is lost, resulting in a slab of thickness 2000 lattice spacings with an interface running through its middle[12]. The slab does, however, retain its periodicity in the x-direction, with a period of 2000 lattice spacings. We will perform simulations of cracks of three nominal lengths, $2a = 181$, $2a = 81$ and $2a = 21$, all with cohesive zones extending ahead of the physical crack for an additional 20 atom pairs. Within the cohesive zone, nonlinear cohesive forces act across the cleavage plane between the two sublattices. That is, these cohesive forces close the crack to form a physical crack tip and core region. The nominal lengths listed above will be corrected in actual cases for the position of the physical crack tip within the cohesive zone, in order to obtain the actual crack length. The long crack is still less than 10% of the super cell size, where we begin to pick up corrections from interactions between cells (see below), and the short crack size is about at the limit below which lattice effects could become significant, relative to the continuum elastic predictions.

The simplest loading configuration is to load the free crack at its center, however, even then the factor $(a+t)/(a-t)$ in the continuum equations must be kept in mind, because the actual crack tip is not at the start of the cohesive zone. (See below.)

A very important consideration in all our work will be the fact that we study **equilibrium** cracks. That is, the crack configuration will be in complete static equilibrium under the action of the external loads, and the atomic bonding forces in the core region at its tip. In the mechanics and elasticity settings, one speaks of Mode II or Mode III cracks, where there is no opening load. Such cracks would not be in the static equilibrium we assume here. The physical requirement that the crack be in rigorous static equilibrium has crucial consequencies for the conclusions we will draw.

5 Lattice Results.

5.1 The Transition Layer.

The lattice analogue of the pure abrupt interface is that where the bonds between the two interfaces have the same spring constant as one of the two sublattices. However, physically, there is no reason why the bonds between the two different atoms facing one another across the interface should have the same properties as the bonds within either of the sublattices. That is, one expects that a transition region between the two will develop with its own interfacial characteristics. In our simulations, we can control the interface bond independently of the sublattices, and we explored the effect of making the interface spring constant the same as one sublattice or the other, and for the case where it was midway between. We found only negligible differences of only a few percent in crack properties for all cases, so we shall standardize on the following choice of spring constants, unless noted otherwise: $c_1 = 1$, $c_2 = 2$, $c_{12} = 1.5$, where the subscript (1) refers to the lower half crystal, (2) the upper, and (12) the interface bond. Because of the scaling properties of the system, we shall always choose $c_1 = 1$, even when other choices are made for the other constants.

Figure 3 shows the result of a simulation, using the above assumptions. It depicts only the double row of atoms on the cleavage plane in the cohesive zone (plus one). Specifically,

the twenty pairs of atoms on the right in the figure represent the atoms facing one another across the cleavage plane, to which bonds may be attached. The first atom pair on the left is the first atom pair on the open crack to which bonds are never attached, and is plotted to assure the reader that the solution is smoothly varying between the unattached atoms of the open crack and the atoms of the cohesive zone where they may be attached. The solid circles represent the normal atomic size, and the second circle about each atom shows the range of the force, such that when the outer circles around two atoms do not overlap, there is no force between the atoms. The shade of the inner circle indicates the magnitude of the force exerted on the atom from atoms within its range across the cleavage plane. Black indicates zero force; white, maximum force. We consider the crack tip to be at that atom pair where the force is maximum. Thus, the physical crack tip shown is not the first atom pair in the cohesive zone, but the second (i.e. the third atom pair from the left because the first pair is outside the cohesive zone). In all our results, we shall compute the actual crack length by taking account of exactly where the physical crack tip is, but we will often refer to a nominal crack length, which is simply the length of the total crack less the cohesive zone. Labels on the figure give the various crack parameters.

5.2 Mode Phase Shifts in the Core.

The phase shift, ξ_0 of Eq. (8), is the most critical property of the interface crack, and we begin our study of the atomic details by exploring how ξ_0 can be defined in terms of a shear–neutralized core. From this exploration, a first definition of the effective core size follows.

Figure 4 is a graph of the relative shear displacements between corresponding atoms on the upper and lower cleavage plane in the cohesive zone (plus one); i.e. the curve is plotted from the atom positions displayed in Fig. 3. Two cases are shown. One is for pure Mode I loading, and the second is for the neutralizing Mode II load which as closely as possible cancels the shear load at the first atom in the core. We can calculate the predicted value for this critical neutralizing load from the elastic continuum equations, by setting the imaginary part of Eq. (8) to zero, i.e. $k_{II} = 0$. Under this condition, the predicted value of the ratio of Mode II to Mode I loads, is given by

$$\frac{F_{II}}{F_I} = \tan\xi_0 = \tan\Big(\epsilon \ln(r_0/2a)\Big). \tag{17}$$

In this equation, we have neglected the small terms which come from the phase effects in the factor in $((a+t)/(a-t))^{i\epsilon}$ in the definition of K in Eq. (1). In our simulations, t is small enough that the approximation in Eq. (17) is excellent. We display the results in Table I for a nominal crack length of $2a = 181$. Columns 3 and 4 show the observed load values, and column 5 shows the load ratios. In column 6, we use Eq. (17) (and Eq. (8)) to calculate the values of r_0 which fit the observed load ratios. The computed core sizes are much smaller than the physical core size, showing that the observed mode shifts in the core are much larger than expected. (Although the effective core size for the modified UBER is nearly half a lattice spacing, the actual physical size of the core in that case is several lattice spacings.)

From the table, there exists a significant difference between the lattice results and the continuum predictions, with the lattice showing much larger mode converted shear at the

tip than predicted by the continuum analysis. We note that the two different force laws also yield different results, and return to this point in a following paragraph.

TABLE I

Neutral Core

$2a = 181$ $c_2/k_1 = 2$ $c_{12}/k_1 = 1.5$ $\alpha = 0.1867$ $\beta = 0.05333$ $\epsilon = 0.04$

	c_{12}	c_2	F_I	F_{II}	F_{II}/F_I	r_0
Gaussian	1.5	2.0	6.0	-1.70	0.2833	0.182
UBER	1.5	2.0	6.1	-1.45	0.238	0.535

The dependence of the shear on distance from the tip is also available from Fig. 4. It visibly decreases with distance from the tip as predicted, but most of that dependence is from the $1/\sqrt{r}$ in Eq. (2). In Fig. 5 we show the elastic values of the shear ahead of the crack from Eq. (1) and compare them with the computed results, both for pure Mode I loading. We have been careful in Fig. 5 to use the elastic shear predictions for the finite crack, because the finite crack stress for distances of 20 or more lattice spacings from the tip differ significantly from the asymptotic results of Eq. (2). The figure shows that the stresses in the core are two to three times those predicted by elasticity, but that the atomic crack values approach the elastic shear values quite accurately at large distances from the core. (We have determined that at the end of the cohesive zone the ratio between the predicted and computed shear stress is 0.9, which is excellent asymptotic agreement at that distance.) Parenthetically, this asymptotic agreement between predicted and computed stresses on the cleavage plane means that the continuum K concept is well preserved in the lattice. In these graphs, the elastic crack tip was taken to be the first atom pair where the force is non zero—not the atom pair of highest force. There is thus a shift of the effective elastic crack tip from the tip one would pick on physical grounds. We note here that the large stresses in the core are propagated well outside the actual nonlinear core region into the linear region. At first glance, these large stresses are surprising, as one expects the elastic core to have larger stresses than the nonlinear core. One can interpret these results in the following way. Suppose we enclose the elastic singularity with an inner circle on which stresses from the actual atomic core are exerted. In the elastic problem with such an internal surface surrounding the core, there will be additional terms of order $r^{-3/2}$ in the Laurent expansion of the elastic potentials for the crack. The actual core is found to be considerably broader than the elastic core, and throughout this core, the atomic forces are near their maximum value. Thus, the stresses at the inner circle are larger than the normal elastic crack solution there, but the elastic stress distribution asymptotically decays to the dominant K–field solution relatively quickly, once the linear region is reached.

The small ξ_0, and related large predicted phase shift in the core have a physical explanation in terms of the nonlinear forces of the core. These nonlinear forces lead to a more compliant core region than predicted by linear elasticity. Thus, for a given stress level in the core, the shear strain is larger than expected, which in turn leads to a larger core shear strain. Finally, the large core strain is then parametrized in the elastic theory

as a small core elastic cutoff parameter, ξ_0.

The shear in the core is also a function of the total crack length, as predicted in Eq. (8). We have explored this functionality, first, in an extreme case, where a large difference exists between the two sub lattices, i.e. $c_1 = 1.0$, $c_{12} = 1.0$, $c_2 = 100.0$, in order to explore the maximum phase angle dependence in the function, $\sigma_{22} + i\sigma_{12}$, at the crack tip. We show the equilibrium configuration for this case in Fig. 6a for pure Mode I loading, with nominal crack length $2a = 21$. The figure shows that the atoms on the top layer (part of the stiff sublattice) are not strained, and that all the strain is in the soft layer on the bottom. The shear now is quite large in the core—in fact, near to lattice breakdown. As the crack length is increased, the core of the crack does break down, and when nominal crack length, $2a = 101$, a dislocation is produced on the cleavage plane, Fig. 6b. We will explore dislocation effects, per se, in the next section. Here, we simply note that the lattice is not able to sustain the shear at the crack tip which the mixing of modes at the crack tip produces, even when the load is pure Mode I. One would like to compare the neutralization shear load for this case, as we did earlier, but the atomic configurations in the core are not so easily interpreted for the extreme mismatch case. The shear varies rapidly, and with the added complexity of the nonlinearity, we are not able to determine a unique neutralized state.

The quantitative exploration of the crack length dependence is more easily determined for the modest mismatch case where $c_2 = 2$ and $c_{12} = 1.5$. In Fig. 7, we show plots of the neutralizing ratio, F_{II}/F_I for three nominal lengths of crack, from $2a = 21$ to $2a = 181$. We also plot curves of Eq. (17) with r_0 picked to make the curve go through the long crack values. The values of core size to provide a fit in each case were drawn from Table I: Gaussian, $r_0 = 0.182$ and UBER, $r_0 = 0.535$.

In both cases, the fit is surprisingly good for the two longer cracks. The short crack result is expected to deviate from the elastic case, and does so in a reasonable direction. The smaller effective core size for the Gaussian law is also expected, because it is shorter range, and gives rise to a smaller physical core size, as well.

In summary, the lattice results show that the qualitative elastic prediction of a mode shift in the core is correct, but the effective core size to achieve numerical correspondence between atomic and elastic results is about an order of magnitude less than the physical core size. The asymptotic form of the phase shift as a function of the distance from the crack tip (Fig. 5), and as a function of crack length (Fig. 7) both conform with the elastic predictions.

5.3 Griffith Criterion Under Mixed Mode Loads.

Our results for the Griffith criterion are displayed in Table II. The first two columns give the model parameters for the loads. $\mathcal{G}_{Ic}$ is calculated from Eqs. (8) and (9) with the effective values of the core size, r_0, taken from Table I for the two different force laws. The surface energy is $\gamma_s = E_b$. In the last column, we present the total classic crack extension force, $\mathcal{G}$, as given in Eq. (4). Values are given for the neutral point, the pure Mode I load point, and for the extreme values of F_{II} where the lattice breaks down. Lattice trapping is significant for the Gaussian force law, but not for the Modified UBER. For this reason, we have two rows for the neutral point for the Gaussian, for the upper and lower trapping points. The trapping at the extreme values for F_{II} disappears, so only one set of values

for Max F_{II} and Min F_{II} are given. For the Modified UBER, the difference in upper and lower k_{Ic} was about 1%, and is neglected. A perusal of the results shows that there is a marked shift of the loads for the critical Griffith state, and that the addition of positive F_{II} increases the F_I required for cleavage. For negative F_{II}, the result is the opposite. Thus, qualitatively, the phase shifts at the crack tip are in the right direction as predicted by the continuum elastic results. However, there are very interesting quantitative features.

First, the values for $\mathcal{G}$ in the last column are intriguing. The classical fracture mechanics argument is that $\mathcal{G}$ should be constant, and equal to the surface energy. The actual values at equilibrium are not constant, and show a minimum in the vicinity of the neutral point.

Our proposal to associate the Griffith relation with the properties of the tension load at the core, and with k_{Ic}, appears to fare rather well, though with some deviation from a simple application of Eq. (9). $\mathcal{G}_{Ic}$ has a maximum value in the vicinity of the neutral load, and is equal at that point to the value of total $\mathcal{G}$. $\mathcal{G}_{Ic}$ significantly deviates from its maximum value, however, when shear stresses are present in the core. This behavior is exactly what we found in the lattice studies for the homogeneous lattice[15]. In that case, also, we found that the crack stability line was curved, with a maximum value of k_{Ic} for pure Mode I.

The Griffith value for the neutral point is roughly 15% above the theoretical neutral point and the critical values of k_{Ic} are too high by about 7%. The reason for this is that the crack length is beginning to get beyond the infinite approximation which we have used. That is, the crack is beginning to interact with the free surfaces, and the other cells. When we decrease the crack size to 81 from 181, the Griffith prediction for $\mathcal{G}_{Ic}$ comes to within about 6% of the theoretical infinite crack result. Knowing this, we continue to give results for the long crack, but the reader is cautioned that predictions for critical values of k are going to be high by about 7% in all cases.

TABLE II

Griffith Relation Under Mixed Mode Loading.

$2a = 181$ $c_2 = 2$ $c_{12} = 1.5$ $\alpha = 0.1867$ $\beta = 0.05333$ $\epsilon = 0.04$

	F_I	F_{II}	$\mathcal{G}_{Ic}$	$2\gamma_s$	$\mathcal{G}$
	Gaussian Force Law. $r_0 = 0.182$ $\xi_0 = 0.2761$				
Max F_{II}	6.20	+2.50	0.0645	0.08	0.104
Min F_{II}	4.40	-4.65	0.0702	0.08	0.0951
Neutral Load$^+$	6.50	-1.70	0.105	0.08	0.105
Neutral Load$^-$	5.60	-1.70	0.0795	0.08	0.0794
Mode I Load	6.2	0.0	0.0825	0.08	0.0892
	UBER Force Law. $r_0 = 0.535$ $\xi_0 = 0.2333$				
Max F_{II}	6.20	+1.70	0.0738	0.08	0.0959
Min F_{II}	4.95	-3.85	0.0756	0.08	0.0912

Neutral Load	6.1	-1.45	0.0912	0.08	0.0912
Mode I Load	6.2	0.0	0.0845	0.08	0.0892

We associate k_{Ic} with the necessary condition for existence of an equilibrium crack[15,16], and the total $\mathcal{G}$ with the energy absorbed when a such a crack moves during a state of mixed load. The fact that $\mathcal{G}$ is a minimum at the neutral point shows that energy conservation is satisfied in such a picture. If a crack under mixed load in the core satisfies the equilibrium condition, then it will accelerate under the excess driving force supplied by $\mathcal{G}$. That is, such a crack would accelerate to high speed as soon as it is created. (In our computer simulations, we load under a decreasing K configuration, so this unstable run–away condition does not occur, even when lattice trapping is small.)

5.4 Dislocation Emission and a Second Definition of ξ_0

We have already mentioned dislocation formation on the cleavage plane in terms of the lattice breakdown limits for the Mode II shear in the core. This emission is depicted in Fig. 8 for both positive and negative dislocations. The figure shows the critical point just before the dislocation is emitted, and indicates both Mode I and Mode II loads for these critical values. The simulations are shown for the modified UBER force law, with the standard parameters used earlier.

We will interpret these results on the basis of Rice's unstable stacking fault criterion[14], Eq. (10). Based on this idea, the emission criterion expressed in terms of the local core k_{II} should be symmetric about zero, because of the symmetry in the unstable stacking fault itself, for this lattice. In the homogeneous lattice[15], we did, in fact, observe strict symmetry relative to positive and negative dislocation emission. However, if we use the definition of ξ_0 defined in §5.2, which was successful in explaining the Griffith condition in §5.3, we would find an asymmetric emission condition in the local stress intensity axes. That is, k_{IIe} for positive disloction emission would not be the same as k_{IIe} for negative emission. This result implies that the choice of ξ_0 may be incorrect, and this suggestion is confirmed by the physical results in Fig. 8 that the core of the crack just before shear breakdown is considerably different, and larger than the neutral core of §5.2. That is, the dislocation emission criterion must be specified in terms of a different effective core size than that which charaterizes the neutral core. Thus, in this section we define a second ξ_0 and effective core size, such that the dislocation emission is symmetric in the local stress intensity factors.(The reader is reminded that the midpoint of the range between the emission of the positive and the negative dislocation is not a neutral core. Thus, the physics of the emission process, in this respect, is not what one would expect, a priori.)

TABLE III

Dislocation Emission.

2a=181 $c_2/c_1 = 2$ $c_{12}/c_1 = 1.5$ $\alpha = 0.1867$ $\beta = 0.05333$ $\epsilon = 0.04$

	F_{Ie}	F_{IIe}	ξ_0	r_0	k_{IIe}	$\mathcal{G}_{IIe}$	γ_{us}
Gaussian Force Law.							
Max F_{IIe}	6.20	+2.50	0.200	+1.22	0.217	0.0328	0.0363
Min F_{IIe}	4.40	-4.65	0.200	-1.22	0.217	0.0328	0.0363
UBER Force Law.							
Max F_{IIe}	6.20	+1.70	0.191	1.55	+0.168	0.0195	0.0221
Min F_{IIe}	4.95	-3.85	0.191	1.55	-0.168	0.0195	0.0221

Our results are shown in Table III, with some of the same parameters already displayed in Table II. The first two columns correspond to load values at the maximum and minimum points. The third and fourth columns give the new values of ξ_0 and r_0 for emission as discussed above. The remaining columns give the derived k_{IIe}, $\mathcal{G}_{IIe}$, and the relaxed γ_{us}[14,15] for the interface. Specifically, the γ_{us} calculation is performed by shearing two blocks of material past one another (relaxed in the tensile direction), with force laws corresponding to the interfacial bonds.

The results of the table show that the Rice criterion for emission is satisfied at roughly the 10% level—a remarkably accurate prediction, in our opinion. The fact that the atomic results are somewhat lower than the prediction is probably not significant.

It is disappointing that the core size is not a unique quantity for the crack problem, but the atomic results show clearly that the structure of the core changes with the amount of shear present, and that the size is larger near lattice breakdown than near the neutral point. Compare Figs. 3 and 8. In view of this physical result, it is expected that the effective core sizes should also be significantly different.

The core sizes and structure also depend on the form of the force law, as one would expect. The fact that the atomic emission criteria track quite accurately the very different values of the unstable stacking fault for the two different force laws is very satisfying.

The discussion in this section has focussed on the physics of the crack core. From the more phenomenological and macroscopic point of view of the applied loads and the K picture, we see that as the crack grows in length under pure mode I load, it becomes increasingly easy to emit positive dislocations, more difficult to emit negative dislocations, and at a critical length, spontaneous positive dislocation emission begins to take place.

6. Conclusions.

By extending the elastic equations in physically reasonable ways, we find that a simple picture of interfacial cracking can be constructed which is consistent with lattice calculations carried out with an interface in a hexagonal lattice. This physical situation can be graphically displayed in a crack stability diagram with two sets of K–space axes. One set of axes is the stress intensity localized at the crack core, and the other set is the applied stress intensity. The stability of the crack is determined by the local stress intensity, and the load point axes are rotated relative to the former by the angle, ξ_0.

The Griffith condition in terms of the local core stress intensity factor, k_{Ic}, and the effective core size is satisfied when account is taken of the finite cell size of the system. There is a small dependence on Mode II, as in the homogeneous lattice case, but this Mode II dependence is not the quadratic dependence given by the standard continuum mechanics total $\mathcal{G}$ in Eq. (4)[15].

The unstable stacking fault criterion for dislocation emission is not satisfied with the effective core size computed from the neutral point in the core, because the emission is not symmetric about zero k_{II}. If a different effective core size is defined such that the emission is symmetric, then the unstable stacking fault criterion for emission is satisfied surprisingly closely.

The picture presented here in terms of the crack stability diagram is appealing in its physical simplicity, and, furthermore, the quantitative aspects of interfacial fracture can be parametrized by the lattice theory. However, the core size of the crack is not a unique quantity, but depends on the amount of shear in the core. This physical result is also reflected in two effective core sizes in our work—one for the description of the shear distribution near the neutral point and another for dislocation emission when the core breaks down in shear. Both definitions of effective core size yield values which are smaller than the physical core, and the first definition is about an order of magnitude less. These small effective core sizes mean that the mode shift for the physical crack is much larger than one would expect on the basis of the linear elastic theory.

Thus for any specific material, and for a specific core–sensitive process, the effective core size must be determined by considerations which lie beyond linear elasticity.

We therefore believe that it would be a very useful excercise to return to the more sophisticated continuum models of crack/dislocation structure typified by the approach of Achenbach, etal[10] for the pure interfacial crack and of Beltz and Rice[17] and Anderson, etal[18] for the dislocation emission problem. In these more extended elastic approaches, it might be possible to get a semi–quantitative understanding of the large phase shifts we have found in the lattice modeling.

Figures

Fig. 1. Crack configuration in the hexagonal lattice used in the atomic simulations. The orgin is at the center of the crack. The lower lattice is connected by springs of strength c_1 and the upper lattice is connected by springs of strength c_2. The springs between the upper and lower lattices have springs of spring constant c_{12}. The right side has cohesive forces turned on in a "cohesive zone" in the tip region. The nonlinear bonds are shown as wavy lines. The load is shown as a force dipole acting at the center of the physical crack (i.e. original crack minus cohesive zone).

Fig. 2. Interfacial crack stability diagram. The crack stability is determined by the Griffith relation for the crack in the lattice, limited by the points where dislocation emission occurs. The upper limit is for positive dislocation emission, and the lower for negative emission. These criteria and limits are determined in terms of the local stress intensity axes, k_I/k_{II}. The load point stress intensity axes, K_I/K_{II} are rotated by the angle, ξ_0, relative to the local axes.

Fig. 3. Configuration of the atoms in the cohesive zone of a crack in equilibrium under the action of its bonding forces (modified UBER potential) near the tip with a pure tensile load, $F_I = 6.2$, exerted at the center of the crack. This crack has an open cleavage length of a total of 181 atom pairs extending to the left of the atoms displayed in the figure. The last atom pair of this open cleavage plane is the first pair shown on the left. The remaining 20 atom pairs shown are those in the cohesive zone whose bonding forces are switched on, and will form bonds whenever the distance between any two atoms facing one another across the cleavage plane is within range. The shade of gray depicts the magnitude of force on an atom exerted by atoms across the cleavage plane. Black corresponds to zero force; white to maximum force. The solid circle represents the radius of the atom (equilibrium interatomic distance), and the second open circle about an atom gives the range of the force law (second neighbor distance). The configuration shown indicates a self consistent solution in that the first atom pair, whose bond forces are always turned off are not within force range of any atoms across the cleavage plane. The atom pair defined to be the tip of the crack is that where the force is greatest.

Fig. 4. a) Plot of the relative shear across the cleavage plane for the configuration of Fig. 3, for pure Mode I load $F_I = 6.20$. The nominal crack length is given by $2a = 181$, $c_{12} = 1.5$, $c_2 = 2$, and the force law is the modified UBER with $\alpha = 0.1867$. b) shows the same case with the $F_I = 6.1$ and a neutralizing Mode II load, $F_{II} = -1.45$. The Mode I load had to be modified, in order to achieve the same general core configuration for the equilibrium crack.

Fig. 5. Plots of the shear and tension stresses across the cleavage plane for the crack of Fig. 4a. (Modified UBER potential.) a) The shear stress, computed from the x-component of force transmitted across the cleavage plane for an atom pair, is plotted (dashed line) as a function of the distance from the start of the cohesive zone. We averaged the x–component force for each atom of a pair to obtain the stress. Using the computed k values, the finite crack stress from Eq. (1) is plotted as a full line for comparison. b) A similar plot is shown for the normal tension component of the force transmitted across the cleavage plane. Again, the lattice values approach the full elastic line, asymptotically.

Fig. 6. High mismatch configuration in Mode I. (a) The nominal crack length is only $2a = 21$, with mismatch ratio $c_2 = 100$, $c_{12} = 1.0$, and modified UBER force law with $\alpha = .272$ and $E_b = 0.04$, and yet the equilibrium crack has almost sufficient shear stress in the core to cause lattice shear breakdown and dislocation formation. (b) For $2a = 101$, the crack breaks down with dislocation emission.

Fig. 7. Crack length dependence of shear phase angle. Curves are shown for the shear neutralizing ratio F_{II}/F_I, as a function of total nominal crack length, $2a$. Curves are drawn separately for the two force laws. We have also plotted logarithmic functions as predicted by Eq. (8) to fit the points at $2a = 181$, from which an effective crack core size can be determined. Crack sizes simulated were for $2a = 21, 2a = 81, 2a = 181$.

Fig. 8. Critical configurations for emission of (a) positive and (b) negative dislocations from an interfacial crack. Crack parameters are given in Table III.

References

1. M. L. Williams, Bull. Seismol. Soc. Amer. **49**, 199 (1959).
2. A. H. England, J. Appl. Mech., **32**, 400 (1965).
3. J. R. Rice and G. C. Sih, J. Appl. Mech., 32, 418 (1965).
4. B. M. Malyshev and R. L. Salganik, Inter. J. Frac. Mech., **5**, 261 (1965).
5. J. W. Hutchinson, M. E. Mear and J. R. Rice, J. Appl. Mech., **54**, 828 (1987).
6. J. R. Rice, J. Appl. Mech., **55**, 98 (1988).
7. Z. Suo, Proc. Roy. Soc., **A427**, 331 (1990).
8. H. Gao, J. Appl. Mech., **58**, 931 (1991).
9. M. Comninou, J. Appl. Mech., **44**, 780, (1977).
10. J. D. Achenbach, L. M. Keer, R. P. Khetan, and S. H. Chen, J. Elasticity, **9**, 397 (1979).
11. J. K. Knowles and E. Sternberg, J. Elast., **13**, 257 (1983).
12. R. Thomson, S. J. Zhou, A. E. Carlsson and V. Tewary, Phys. Rev. **B**, **46**, 10613 (1992).
13. J. H. Rose, J. R. Smith and J. Ferrante, Phys. Rev. B, **28**, 1835 (1993).
14. J. R. Rice, J. Mech. Phys. Sol., 40, 239 (1992).
15. S. J. Zhou, A. E. Carlsson, and R Thomson, Phys. Rev. B, **B47**, 7710 (1993).
16. I. H. Lin and R. Thomson, Acta Met., **34**, 187 (1986).
17. G. E. Beltz and J. R. Rice in Modeling the Deformation of Crystalline Solids: Physical Theory, Application, and Experimental Comparisons (ed. T. C. Lowe, A. D. Rollett, P. S. Follansbee and G. S. Daehn) p457. TMS
18. P. Anderson, Shastry and R. Thomson, To be Published.

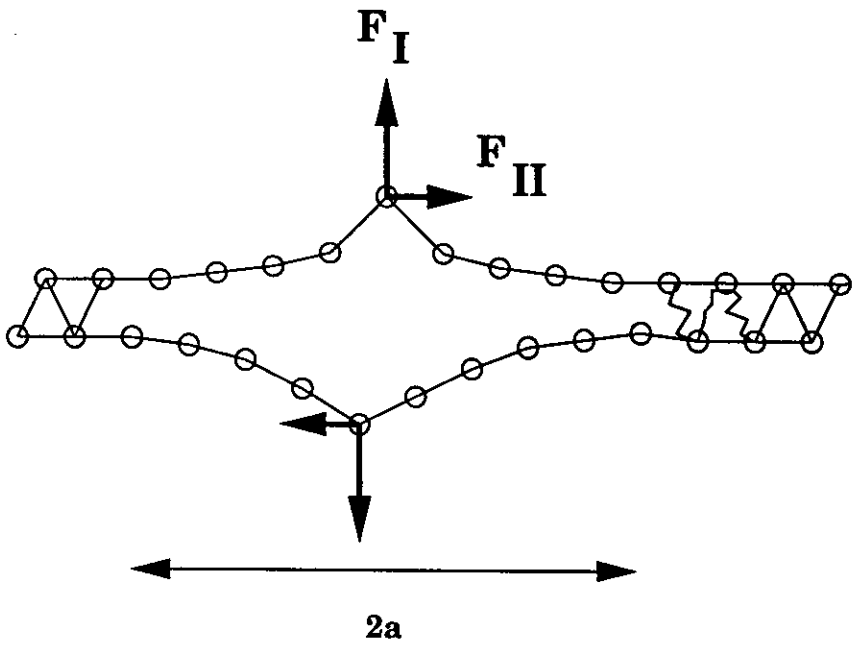
F I
F II
2a

Fig 1

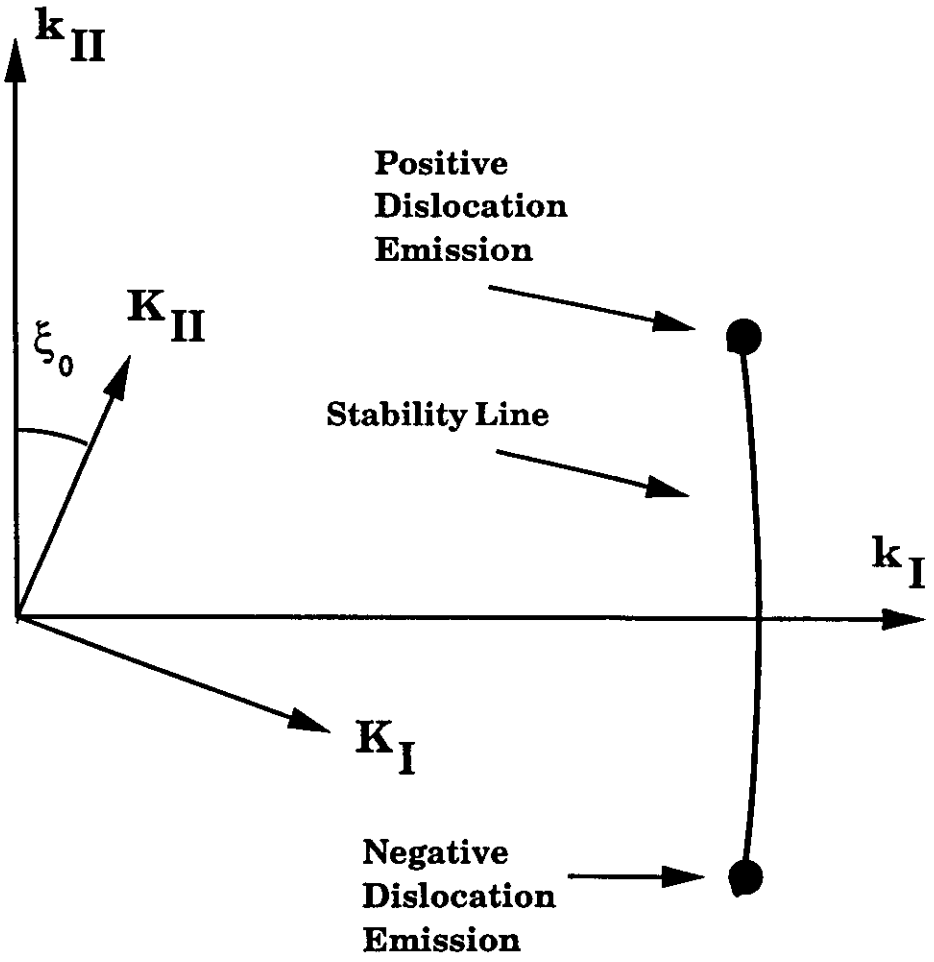
k II
Positive
Dislocation
Emission
ξ0
K II
Stability Line
k I
K I
Negative
Dislocation
Emission

Fig 2

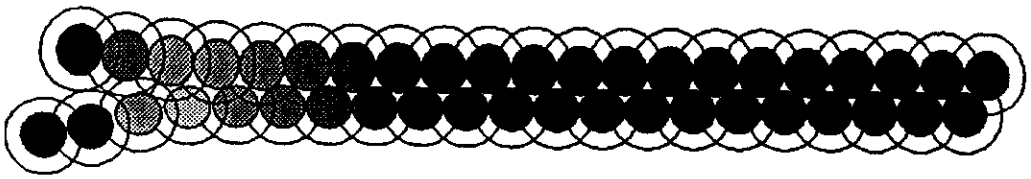

Fig 3

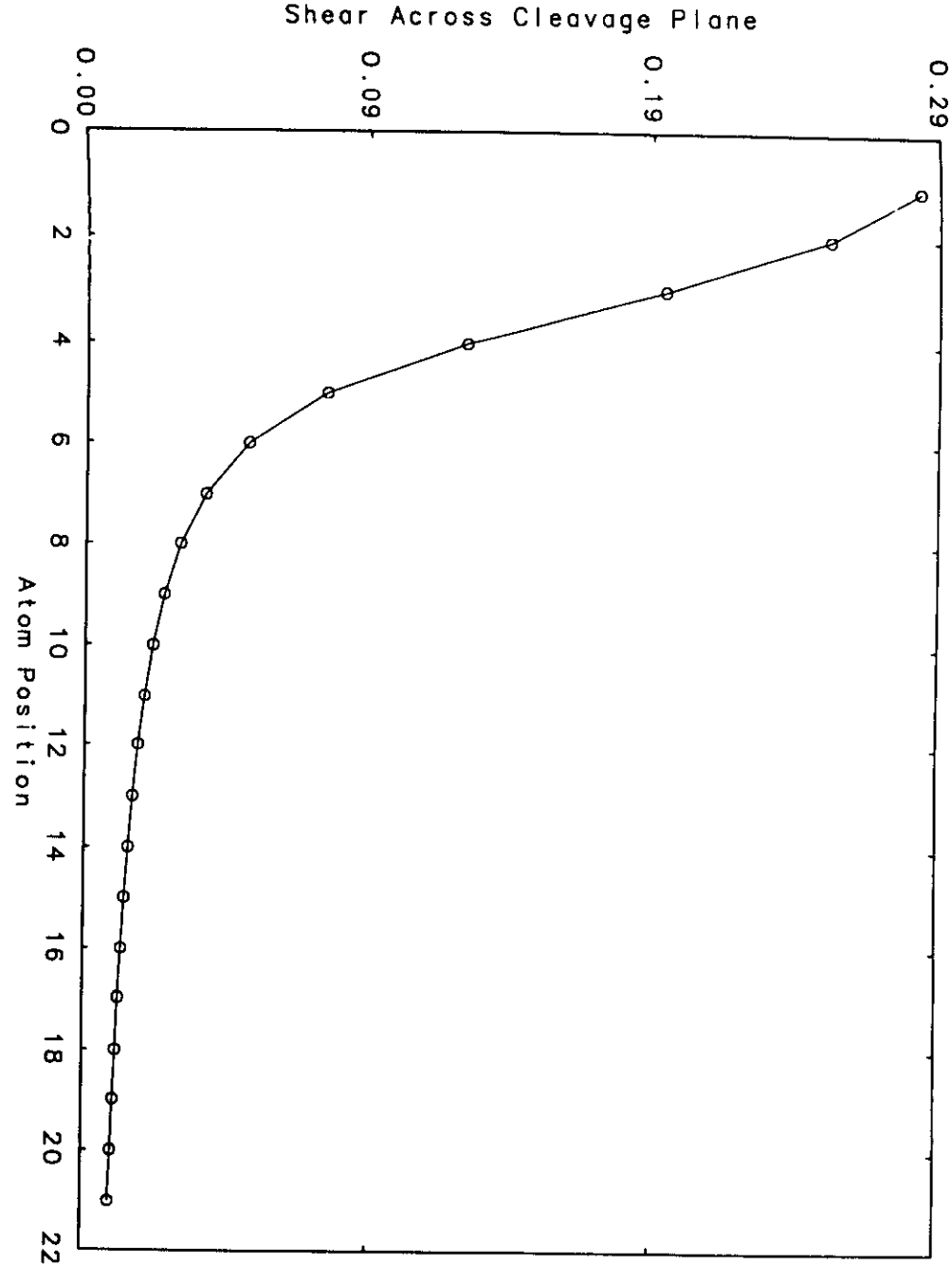
Shear Across Cleavage Plane
0.00
0.09
0.19
0.29
Atom Position
0
2
4
6
8
10
12
14
16
18
20
22

Fig 4a

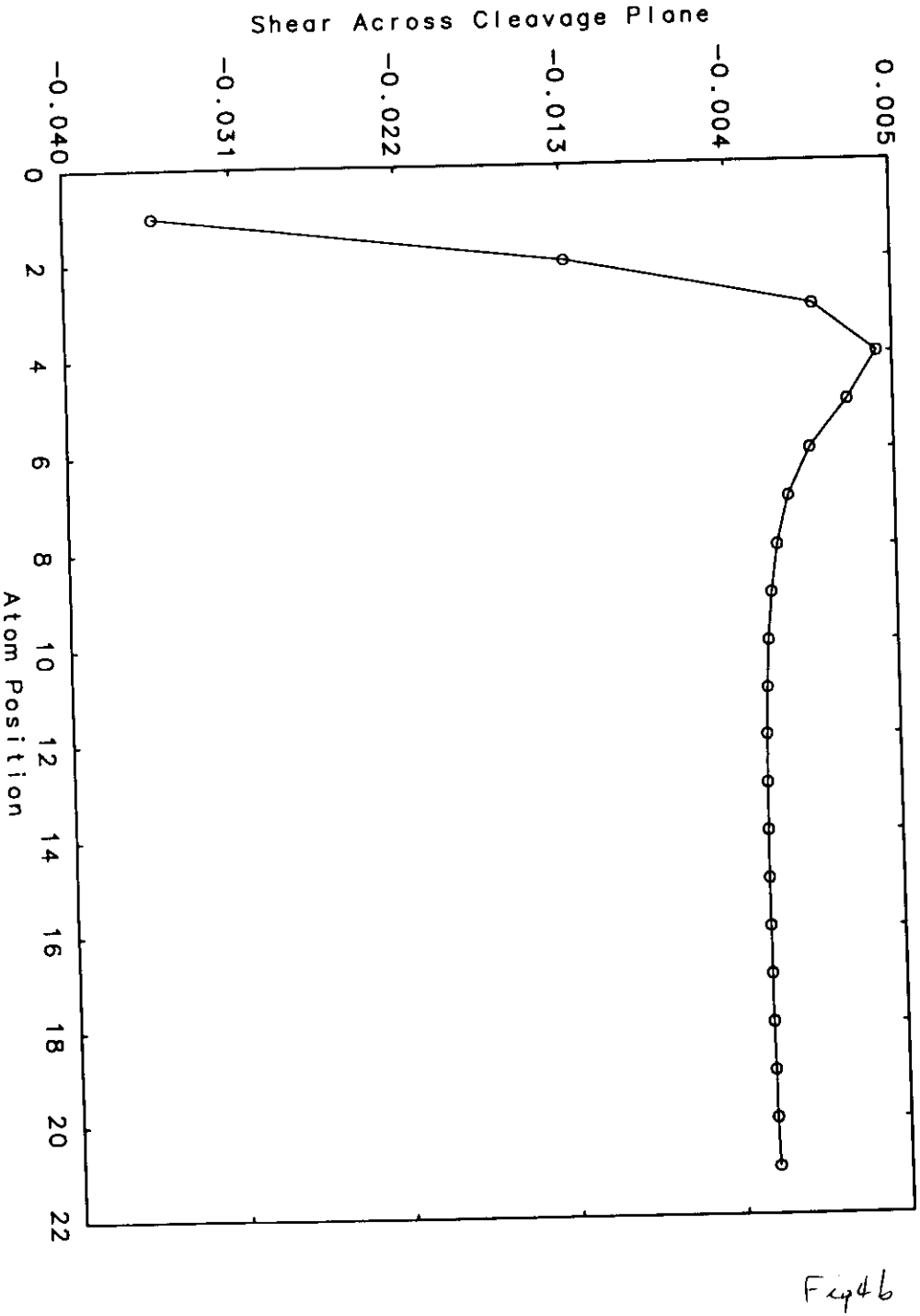
Shear Across Cleavage Plane
-0.040
-0.031
-0.022
-0.013
-0.004
0.005
0
2
4
6
8
10
12
14
16
18
20
22
Atom Position

Fig 4b

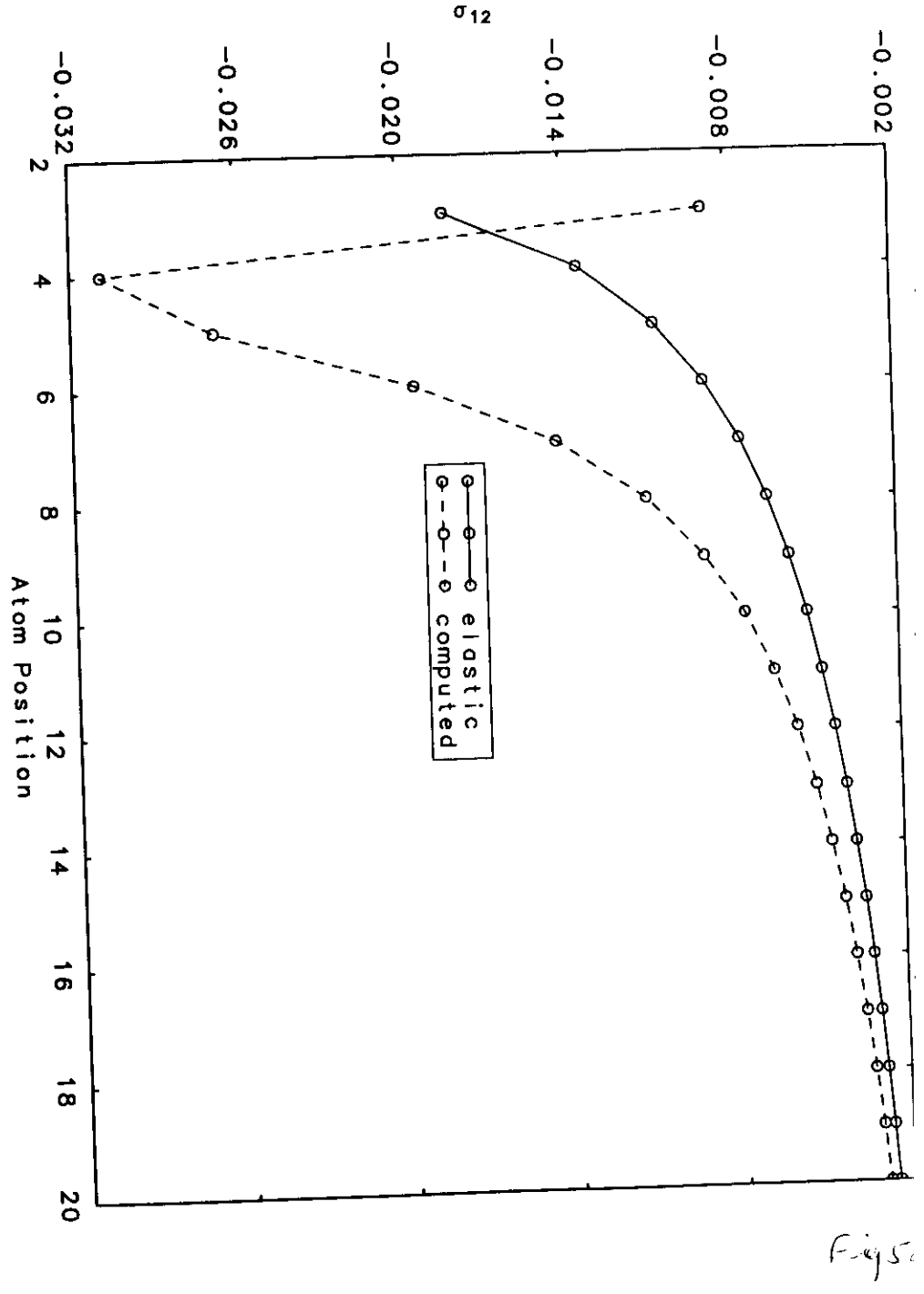
σ_{12}
-0.032
-0.026
-0.020
-0.014
-0.008
-0.002
2
4
6
8
10
12
14
16
18
20
Atom Position
elastic
computed

Fig 5

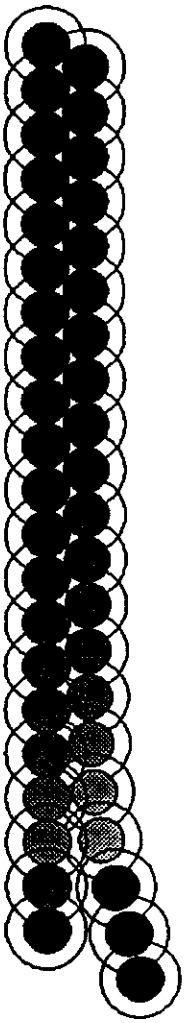

Fig 6

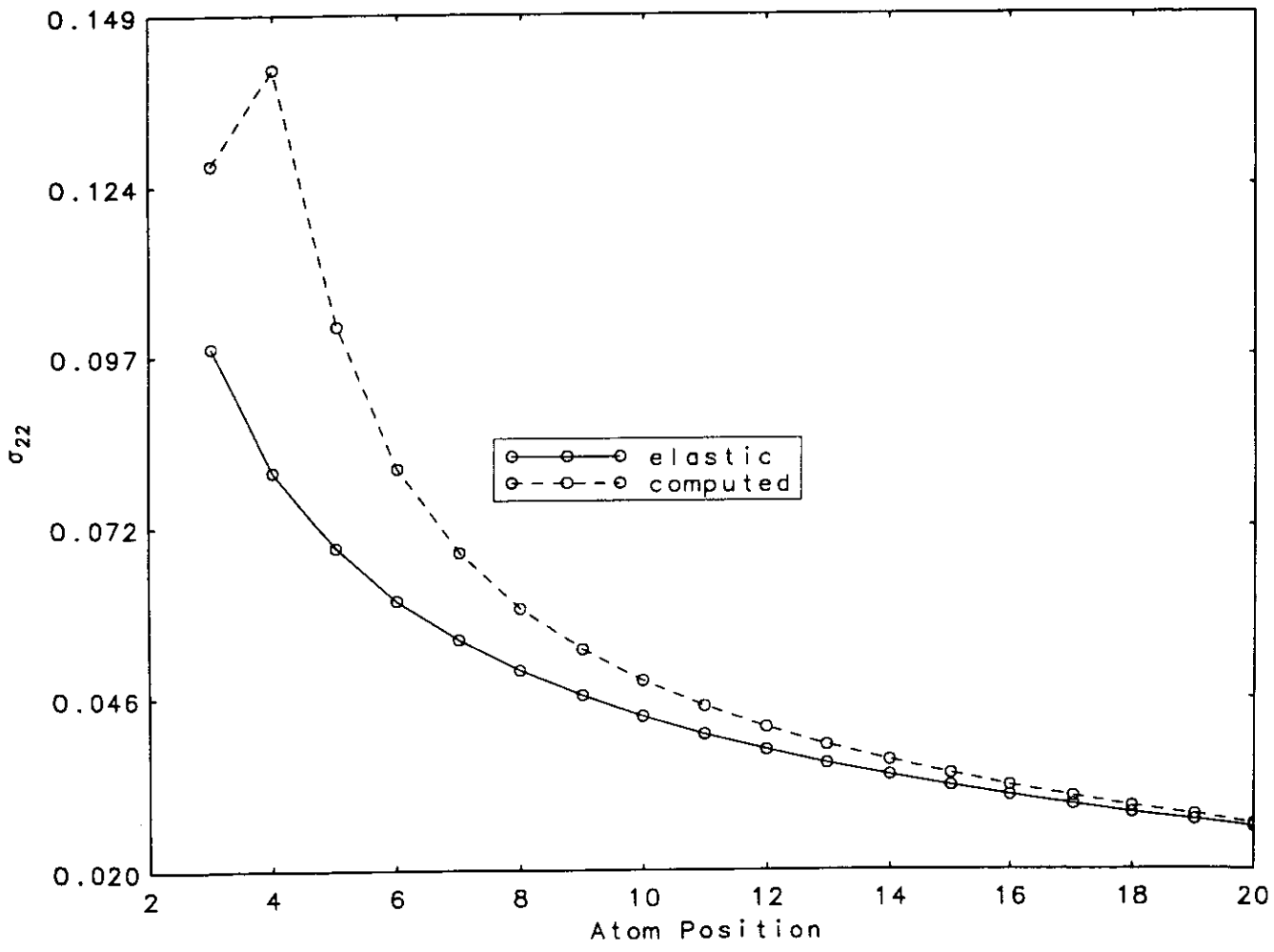
0.149
0.124
0.097
0.072
0.046
0.020
σ_{22}
elastic
computed
2
4
6
8
10
12
14
16
18
20
Atom Position

Fig 5

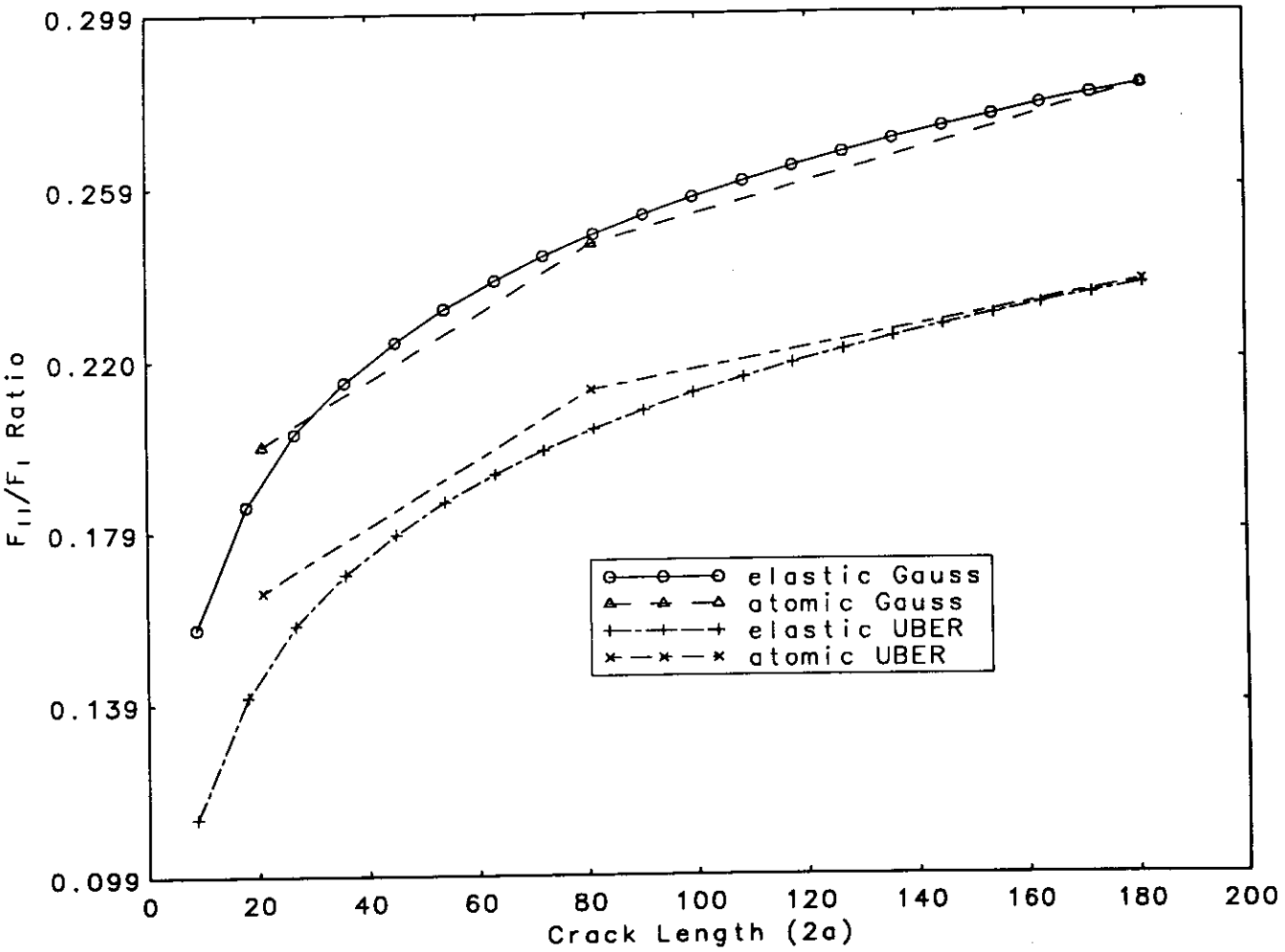
0.299
0.259
0.220
0.179
0.139
0.099
F_{II}/F_I Ratio
0
20
40
60
80
100
120
140
160
180
200
Crack Length (2a)
elastic Gauss
atomic Gauss
elastic UBER
atomic UBER

Fig 9

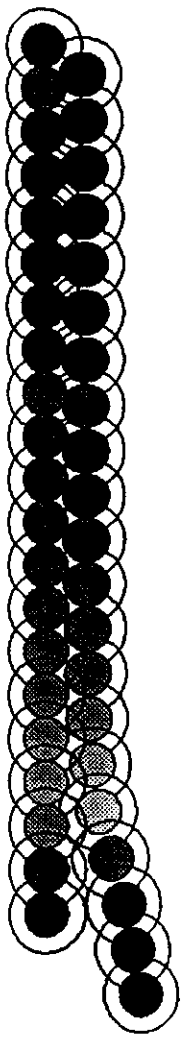

Fig 66

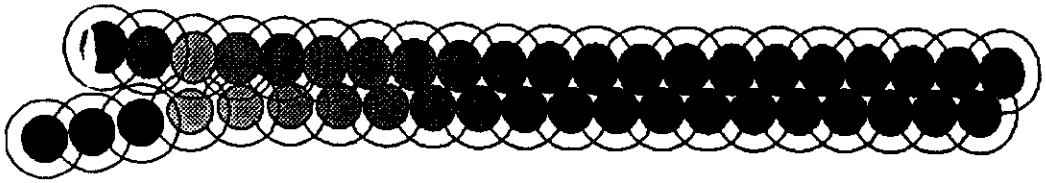

Fig 8a

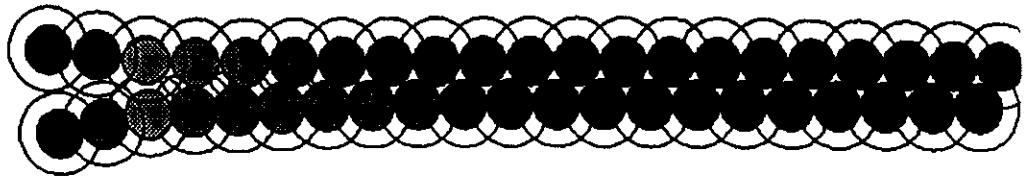

Fig 8